5-2010

In vitro Analysis of Microfluidic Neural Probes

Joshua Kessler
University at Albany, State University of New York

Joshua Kessler

2010

In vitro Analysis of Microfluidic Neural Probes

An honors thesis presented to the

Department of Biological Sciences

University at Albany

State University of New York in partial

Fulfillment of the Honors Program Requirements

Acknowledgements

Nathaniel Cady, College of Nanoscience and Engineering, State University of New York at Albany

Matthew Hynd, College of Nanoscience and Engineering, State University of New York at Albany

Blaze Messer, College of Nanoscience and Engineering, State University of New York at Albany

Department of Biological Sciences
University at Albany

This Honors Thesis has been read and approved
by the undersigned and is hereby recommended for acceptance.

Thesis Committee:

Research Advisor: (Name) _____

(Signature) _____

(Date) _____

Member: (Name) _____

(Signature) _____

(Date) _____

ACTION: Accepted ☐ Not Accepted ☐

_____ _____
Robert Osuna Date

Departmental Honors Program Director

Table of Contents

1. Abstract

The clinical impact of neural prostheses has been inhibited by a lack of functional stability of the devices due to acute and chronic reactive tissues' responses in the brain. However, prosthetic stability could be improved via local drug administration or delivery of siRNA to mitigate the reactive tissues using microfluidic probes. Neural prosthetic probes have been previously developed, but had asymmetric and uneven distribution of fluid delivery to brain phantoms. Therefore, probes with different geometries and fluid delivery pores (holes ranging from 10 to 20 μm) were tested for functionality *in vitro* using a crystal violet/PBS solution. Compound light microscopy and image capture were utilized to record the diffusion of solution from probes into 1% w/v agarose. Solution diffusion was observed for 30 minutes and diffusion radii were observed for all probe geometries and hole diameters, thus confirming probe functionality. With functionality established, solution release from probes was characterized *in vitro* using Texas-Red labeled dextran pumped into agarose brain phantoms (1% w/v) at a constant rate. Fluorescence microscopy with automated image capture was employed to record the release profile of Texas-Red dextran. Release was monitored for 10 minutes and analyzed using Nikon Elements image analysis software. A significant difference in fluid delivery was observed for different probe geometries and hole diameters. The results suggest these novel probe designs could provide a more symmetric and even distribution of local drug or siRNA delivery during intervention treatment of reactive tissue in response to neural prostheses implantation.

2. Introduction

Technologies aimed at extracting information directly from the brain are a key component in prosthetic systems intended to restore sensory or motor function to patients suffering from the breakdown of normal signaling pathways. Establishing a stable Brain-Computer Interface (BCI) provides an alternative signal pathway that allows activity from the brain to be recorded, processed, analyzed, and used to control complex prosthetic and communication systems.[1]However, the insertion of neural prosthetic devices has been found to elicit reactive responses from both vasculature and nervous tissue. Ultimately these responses prevent the successful integration of prosthetic devices into the CNS. Numerous studies have shown that nervous tissue reacts to implanted neural prosthetic devices through a series of events, consisting of immediate-, early-phase, and chronic-responses.[2] The immediate-response (<1 hr) to devices begins within minutes following implantation. By 30 min post-insertion, neuronal soma near the insertion site undergo morphological changes indicative of neural degeneration.[3,4] The early-phase response (1–7 days) is primarily inflammation, and includes damage to neuro-vasculature, activation of mitogen-activated protein kinase signaling cascades in neurons and glia, and activation of resident microglia and infiltrating leukocytes. Reduced cerebral blood flow following device insertion can also initiate a cascade of events leading to ischemia. The resulting hypoxia and hypercapnia can eventually lead to impairment of cellular ionic homeostasis.[5] Initially, astrocytes maintain homeostasis by scavenging potassium and glutamate, however, these cells ultimately assume classic reactive profiles, including hypertrophy and expression of glial fibrillary acidic protein (GFAP) and vimentin.[6] Reactive astrocytes exhibit maximal GFAP immunoreactivity between 3-7 days post-insertion, with reactive cells found to extend as far as several hundred microns from the initial insertion site.[7,8] Activated microglia and foreign body giant cells also contribute to the insulation of implanted devices. The chronic response (>6 weeks) is characterized by a hyper-trophic reaction from reactive astrocytes. This results in the formation of a glial-fibroblastic sheath that functions as a diffusive barrier, insulating the device, and reducing the ability of the device to communicate with surrounding nervous tissue.[4,9] Numerous studies have demonstrated the decrease in the long-term performance of neural prosthetic devices following implantation. In a study by Rousche and Normann of 11 implanted electrodes, only four remained active after 5 months.[10] Similarly, Williams et al. found that of eight implanted electrode arrays, three failed within the first 15 weeks of implantation.[11] More

recently, Nichols et al. have reported a 40% drop in electrode viability over 18 months of implanted devices.[12] In order to develop BCI technology, two intervention strategies have been devised.

Pharmacological intervention via systemic injections or slow release inflammatory agents from polymers has been shown to alter the tissue responses around implanted devices.[13,14] Although systemic injection is an effective and easy intervention, it is not viable over time because of the side effects associated with long-term use of inflammatory drugs. Local drug delivery however will not present such side effects and will reduce the amount of required drug, eliminate the possibility of peripheral metabolism, circumvent the blood-brain barrier, and provide immediate access to target tissue. Channels built into microfluidic probes can provide a means of local drug delivery, subsequently suppressing reactive tissues' responses and stimulating device functional stability.

The other intervention strategy is the utilization of signal interfering RNA, siRNA. RNA interference, RNAi, is mediated by the assembly of a nuclease complex that leads to homologous mRNA degradation. When cells detect dsRNA, Dicer, an RNase III-like enzyme, processes the long duplexes into 20-25 bp siRNAs in what is called the RNAi initiating step. In the effector step of RNAi, the siRNA enters an RNAi specific nuclease complex known as the RNA-Induced Silencing Complex (RISC). The siRNA is unwound, exposing the antisense strand. This strand binds to the complementary mRNA, and the mRNA is cut by RISC in the center region of the guiding siRNA strand, destroying the mRNA and preventing the creation of protein.; knocking down expression of specific genes.[15] Essentially any gene with a known sequence can be targeted based on sequence complementarity with an appropriate siRNA. This makes siRNAs a useful tool for gene function and drug target validation.

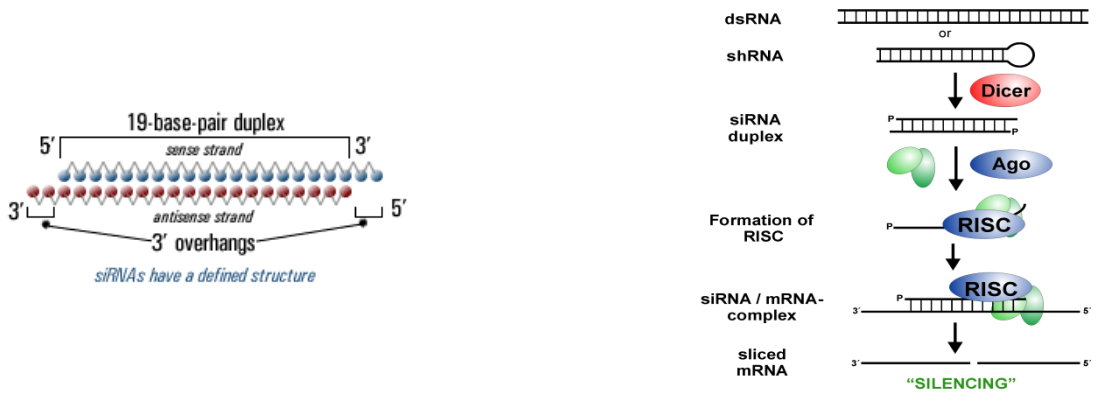

Figure 1. Left panel. siRNA structure. siRNA's are 20-25 bp long dsRNA molecules that have a characteristic two nucleotide 3′ overhang. **Right panel.** Mechanism of siRNA interference. RNAi is a novel strategy for the development of antisense

therapeutics that can result in the potent, long-lasting, post-transcriptional silencing of specific genes. RNAi mechanisms can involve either the degradation of target RNA (short interfering RNA, siRNA), or cause translational arrest of the target RNA (micro RNA, miRNA).[16]

Our experiments with neural probe devices will be performed *in vitro* and as such will not require the use of siRNA. However, another molecule must be used that is safe for use *in vivo* (for data correlation). Dextran is a complex, branched glucan (polysaccharide made of many glucose molecules) composed of chains of varying lengths (from 10 to 150 kilodaltons). The straight chain consists of α-1,6 glycosidic linkages between glucose molecules, while branches begin from α-1,4 linkages (and in some cases, α-1,2 and α-1,3 linkages as well). Dextran is synthesized from sucrose by certain lactic-acid bacteria, the best-known being *Leuconostoc mesenteroides* and *Streptococcus mutans*.[17]

3. Methods and Materials

3.1 Fluidic probe design and fabrication

Microfluidic neural prosthetic devices were fabricated using photolithographic patterning of SU-8 photoresist (Microchem Inc., Newton, MA) using previously-reported techniques.[18] The process flow for fabricating channels in SU-8 polymer has been previously reported by Gracias, *et al*.[18] Briefly, silicon wafers were spin coated with an approximately 50 μm layer of SU-8 photoresist and then photolithographically patterned to establish the base of the devices. A second layer of SU-8, approximately 75 μm thick, was then spun onto the wafer and subsequent lithographic steps were performed to define the sidewalls and topmost (~5μm) covering. The wafer was then developed in SU8 developer overnight to define and release the devices. These process steps are illustrated in Figure 2.

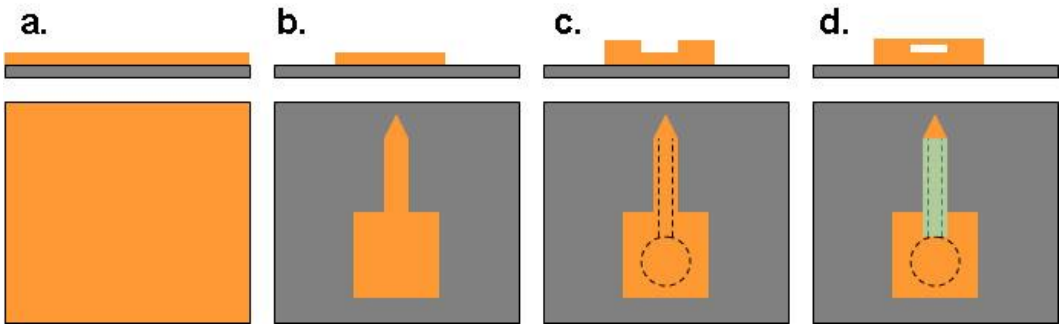

Figure 2. Fabrication strategy for probe devices. A layer of SU-8 photoresist is spin-coated onto a silicon wafer (a) followed by photolithographic pattering of the base of the device (b). A second layer of photoresist is spin-coated onto the wafer and sidewalls (c) and a top layer (d) are defined via photolithographic patterning.

Several different probe geometries were fabricated and tested. Examples of probe geometries are illustrated in Figure 3.

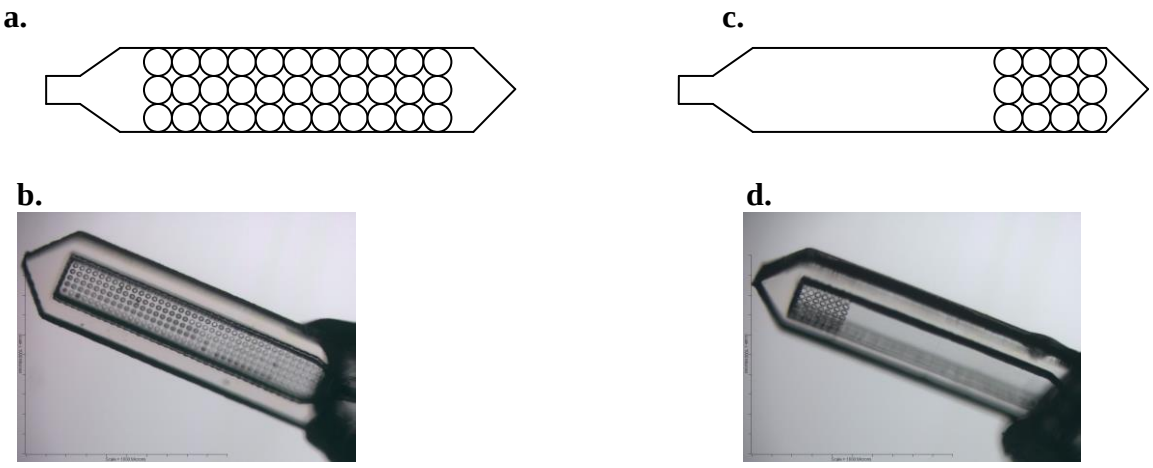

Figure 3. Geometries of fabricated probes. (a) and (b) show a probe with "full-length" geometry, while (c) and (d) show a probe with "tip only" geometry. Images (b) and (d) were captured using a Nikon compound light microscope and Micron software.

3.2 Acute insertion/diffusion system

Fabricated microfluidic probes were inserted into approxiamtely 6 inch long segments of polyimide tubing (Small Parts), with an inner diameter of either 0.020 cm or 0.025 cm, using a stereoscope. Polyimide was used because it is light, flexible, and resistant to heat and chemicals. Gaps between the probe and polyimide tubing were sealed using Super Silicone Sealant (3M, Saint Paul, MN). Once assembled, devices were allowed to dry overnight before use.

To create a staining solution, crystal violet (CV) dye was dissolved in phosphate buffer saline (PBS) to produce a 2% crystal violet solution (CVS). CV is a bactericide and the primary agent used in the Gram Stain Test. It was used in this experiment because of its readily identifiable color. PBS was used in this experiment to maintain a constant pH and the osmolarity and ion concentrations of the solution match those of the human body. Once CVS was generated, it was pumped through 0.1" ID Tygon microbore tubing via a syringe pump (New Era Pump System Inc., Wantagh, NY) to prime the neural probes. Once the probe was primed (fluid observed to be diffusing from probe) the probe was inserted into the 1 % w/v agarose and the syringe pump was shut off. Then, the CVS was allowed to diffuse for 30 minutes into agarose gel. 1% w/v agarose gel was used in this experiment because it most closely resembles the consistency and fluidity of the human brain in vivo. An image was captured every 60 seconds at 4x magnification using a compound-light microscope and Micron software (Micron Technology Inc., Boise, ID). Time was recorded using a digital multi-track laboratory stopwatch.

Once functionality of the probes was established, different geometries and hole diameters (from 10 µm to 20 µm) were characterized using fluorescence microscopy. The probes were assembled as previously described, but with smaller segments of polyimide tubing, approximately 3 inches. A 50 µL Hamilton Co. (Reno, NV) 705N microsyringe loaded with Texas-Red Dextran (TRD) placed in a micron pump was attached to the probes via tygon tubing. TRD was used because its molecular weight mimics that of siRNAs; approximately 3 kDa and Texas-Red is a red fluorescent dye that can be excited by λ= 595-605 nm. With the microsyringe attached to the probe, TRD was pumped to the probes to prime them. Once primed, probes were inserted into agarose brain phantoms (1% w/v) and TRD was pumped at a rate 0.05 µL/minute for 10 minutes. Images were captured every 10 seconds for 10 minutes via automated programming supplied by NIS-Elements Basic Research Elements software and a Nikon Eclipse 80i compound light microscope (Nikon Instruments Inc, Melville, NY). During image capture, probes were exposed to fluorescent light, λ= 595-605 nanometers, for 100 milliseconds with the ND-4 light filter of the microscope on. Data was extracted from the images and imported to Microsoft Excel using the same software. Once imported the data were analyzed and plotted using Microsoft Excel.

4. Results and Discussion

4.1 Initial characterization of fluid delivery from probes

After fabrication of probe devices, with associated microtubing, we sought to evaluate their performance for delivery of fluids into brain phantoms (1% w/v agarose). As described in the methods section, crystal violet solution (CVS) was pumped into brain phantoms while observing the process under bright field microscopy. Images collected during these tests are shown below (Figures 4-5). Figure 4 shows probes with tip-only geometries, while Figure 5 shows probes with full-length geometries. Hole diameter was varied for both full-length and tip-only geometries (reflected in the columns of Figures 4-5). In these figures, CVS can be seen diffusing out of the micropores in these devices, into to the brain phantoms. Diffusion of CVS confirmed probe functionality (i.e., fluid could be released from the micropores and would diffuse into the brain phantom). Images of CVS diffusion were recorded for both geometries tested and of the hole diameters used (10 µm, 15 µm, and 20 µm). Diffusion varied by probe geometry slightly, while diffusion radii varied greatly according to hole diameter (Figures 4-5).

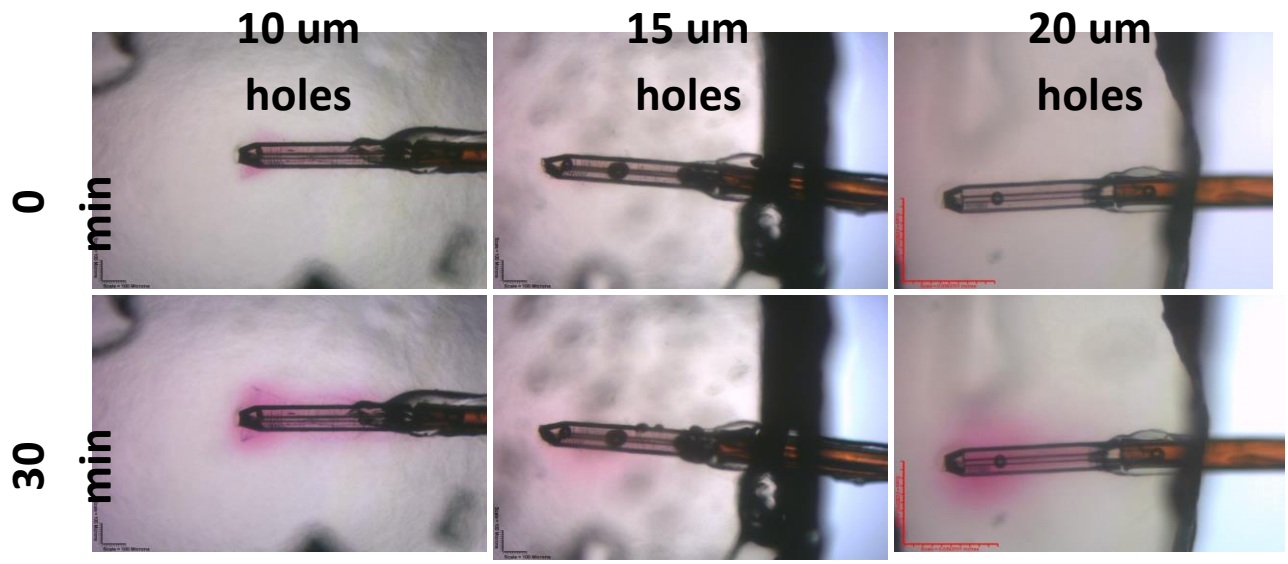

Figure 4. Release of CVS from probes with tip only geometries in agarose brain phantoms (1% w/v). Images from the top row display probes at time of insertion, time = 0 minutes. Images from the bottom row display probes at end of diffusion, time = 30 minutes. Each column represents a probe with a varying diameter of micropores (10 µm, 15 µm, and 20 µm respectively). Images were captured using bright-field microscopy and Micron software. Scale = 100 µm.

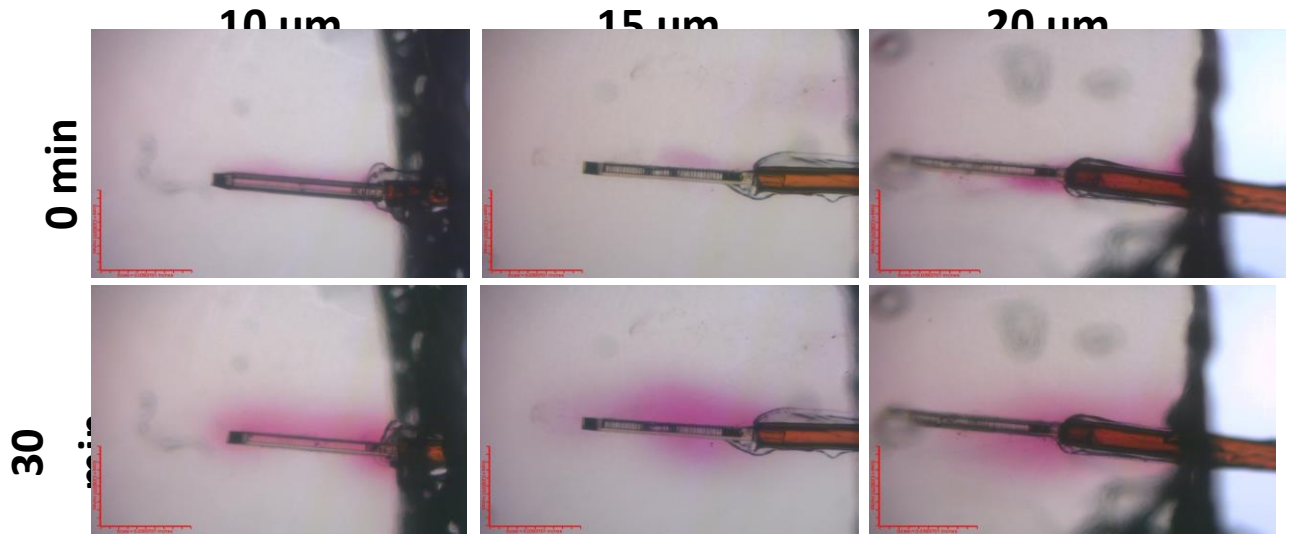

Figure 5. Release of CVS from probes with full-length geometeries in agarose brain phantoms (1% w/v). Images from the top row display probes at time of insertion, time = 0 minutes. Images from the bottom row display probes at end of diffusion, time = 30 minutes. Each column represents a probe with a varying diameter of micropores.(10 µm, 15 µm, and 20 µm respectively). Images were captured using bright-field microscopy and Micron software. Scale = 100 µm.

The results show that the shape of a probe's diffusion radius is more heavily influenced by probe geometry, while the size of a probe's diffusion radius is more heavily influenced by the size of the probe's micropores. Specifically, probes with a tip only geometry tend to have a diffusion radius concentrated on the tip and the middle of the probe, while probes with a full-length geometry tend to have a consistent diffusion radius from the tip to the shank of the probe. It should be noted that in probes with a full-length geometry and either 15 µm or 20 µm pores do not always have a uniform diffusion from tip to shank, because the pores are larger, the diffusion radius does not always reach the probe's tip. This problem was more frequently observed with probes with 20 µm pores versus probes with 15 µm pores. Probes with larger micropores (20 µm) tend to have a larger diffusion radius, while probes with smaller micropores (10 µm) tend to have a smaller diffusion radius. Given this information, it is logical to deduce that a probe with a full-length geometry and either 10 or 15 µm pores will give the most consistent diffusion radius, while probes with a tip only geometry will give a more localized diffusion radius. Additionally, probes with larger micropores will be able to deliver their contents more quickly than probes with smaller micropores. This information may prove useful when considering the target area of drug/siRNA delivery; it is logical to deduce that probes with 20 µm pores would be suited for interventions involving immediate reactive tissue responses, while probes with 15 µm pores would be suited for interventions involving early phase reactive tissue responses, and probes with 10 µm pores would be suited for interventions involving chronic reactive tissue

responses. In an immediate reactive tissue response, tissue reacts to a neural prosthetic probe upon implantation, with minutes. In order to effectively counteract that action, one would want a device that allows for the most rapid delivery of fluid (i.e. a probe with 20 µm pores). In an early reactive tissue response, tissue reacts to a neural prosthetic probe within days of implantation, generally 1-7. To counteract this type of response, one would want a device that allows for moderate delivery of fluid (i.e. a probe with 15 µm pores). In a chronic reactive tissue response, tissue reacts to the presence of a neural prosthetic probe within weeks. To counteract this type of response, one would want a device that allows for gradual delivery of fluid (i.e. a probe with 10 µm pores).

4.2 Quantitative characterization of fluid delivery from probes using fluorescently labeled dextran

Initial experiments with CVS diffusion from neural prosthetic probes gave qualitative information about fluid delivery to brain phantoms. To provide a quantitative comparison among different probe geometries and hole diameters, the aforementioned experimental procedures were modified. Delivery of a fluorescently labeled high molecular weight compound (Texas-Red dextran, 3 kDa), in lieu of CVS, provides a substantial mimic of the prospective drugs and/or siRNA intended for CNS delivery by these devices. Fluorescent labeling of dextran allowed for quantitative fluorescence microscopy and post-imaging analysis (densitometry/intensity–based analysis). For this study, all of the same probe geometries and hole diameters were used (as compared to the CVS study). As described in the methods section, Texas-Red labeled dextran (TRD) was pumped into brain phantoms and successive fluorescence images were collected over a 10 minute period (at a rate of one image every 10 seconds) using automated image capture software; it has been previously determined that 10 minutes is the maximum infusion time for *in vivo* work. Sample images from these experiments are shown below (Figures 6-7).

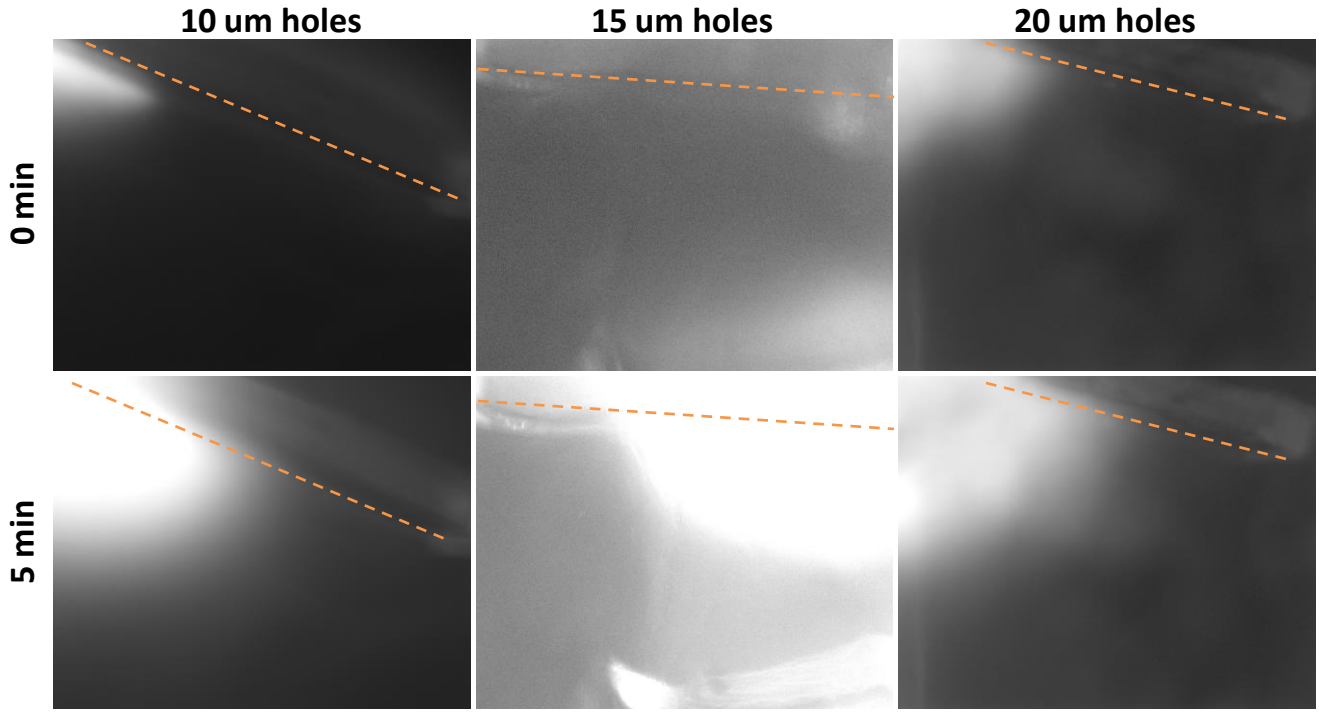

Figure 6. Release of TRD from probes with tip only geometries in agarose brain phantoms (1% w/v). TRD was pumped at a rate of 0.05 µL/minute for 10 minutes. To capture an image, probes were exposed to fluorescent light for 100 milliseconds at λ = 595-605 nanometers. Images from the top row display probes at the time of insertion, time = 0 minutes. Images from the bottom row display probes at the midway point, time = 5 minutes. Orange dotted lines represent the location of the probes in the images. The tip of the probe is on the left side of each image, while the shank (connected with the polyimide tubing) is on the right side. Each column represents a probe with a varying diameter of micropores.(10 µm, 15 µm, and 20 µm respectively). Images were captured using Nikon Elements Basic Research software.

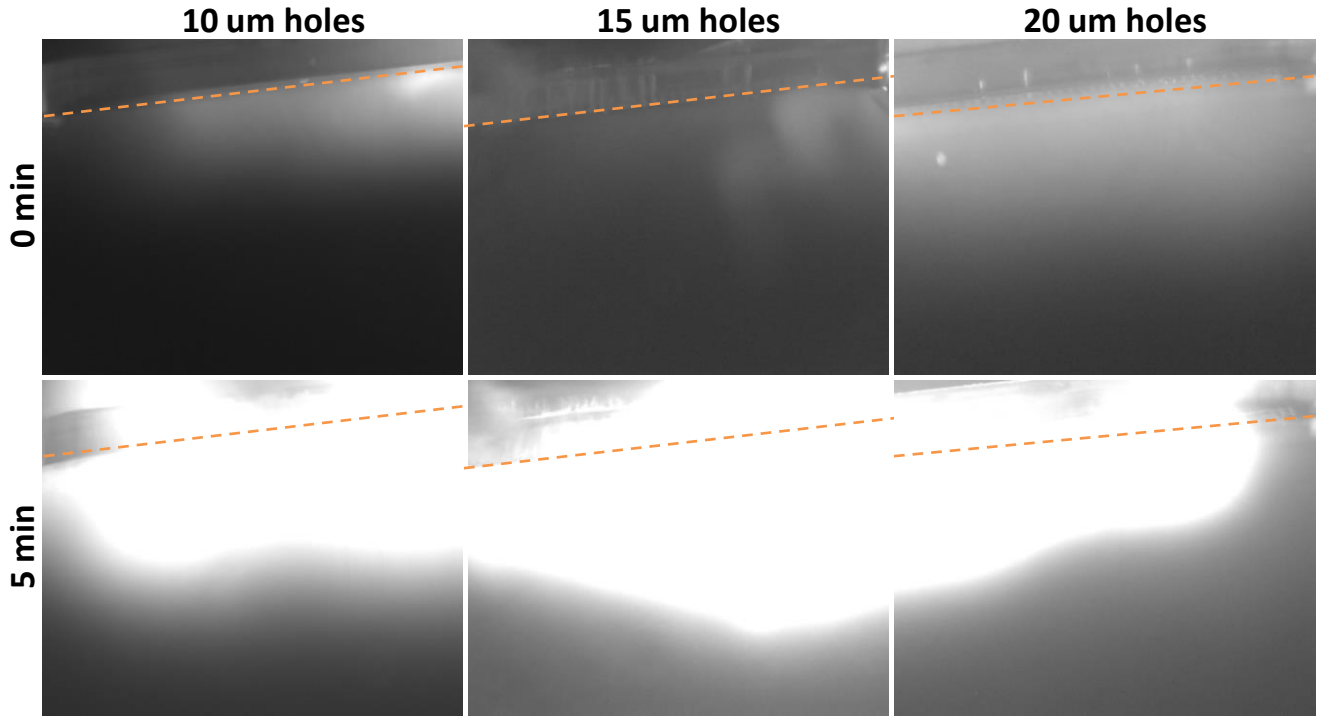

Figure 7. Release of TRD from probes with full-length geometries in agarose brain phantoms (1% w/V). TRD was pumped at a rate of 0.05 µL/minute for 10 minutes. To capture an image, probes were exposed to fluorescent light for 100 milliseconds at λ = 595-605 nanometers. Images from the top row display probes at the time of insertion, time = 0 minutes. Images from the bottom row display probes at the midway point, time = 5 minutes. Orange dotted lines represent the location of the probes in the images. The tip of the probe is on the left side of each image, while the shank (connected with the polyimide tubing) is on the right side. Each column represents a probe with a varying diameter of micropores (10 µm, 15 µm, and 20 µm respectively). Images were captured using Nikon Elements Basic Research software.

These results confirm the findings of the qualitative CVS test; both probe geometries, as well as the three different sizes of micropores are functional in the delivery of solution to agarose brain phantoms. The results show that the shape of a probe's diffusion radius is more heavily influenced by probe geometry, while the size of a probe's diffusion radius is more heavily influenced by the size of the probe's micropores. Specifically, probes with a tip only geometry tend to have a diffusion radius concentrated on the tip and the middle of the probe, while probes with a full-length geometry tend to have a consistent diffusion radius from the tip to the shank of the probe. It should be noted that in probes with a full-length geometry and either 15 µm or 20 µm pores do not always have a uniform diffusion from tip to shank, because the pores are larger, the diffusion radius does not always reach the probe's tip. The problem was more frequent with probes with 20 µm pores versus probes with 15 µm pores. Probes with larger micropores (20 µm) tend to have a larger diffusion radius, while probes with smaller micropores (10 µm) tend to have a smaller diffusion radius. Given this information, it is logical to deduce that a probe with a

full-length geometry and either 10 µm pores will give the most consistent diffusion radius, while probes with a tip only geometry will give a more localized diffusion radius. Additionally, probes with larger micropores will be able to deliver their contents more quickly than probes with smaller micropores. This information may prove useful when considering the target area of drug/siRNA delivery; it is logical to deduce that probes with 20 µm pores would be suited for interventions involving immediate reactive tissue responses, probes with 15 µm pores would be suited for interventions involving early phase reactive tissue responses, and probes with 10 µm pores would be suited for interventions involving chronic reactive tissue responses.

In addition to substantiating the CVS results, the TRD results assert that our probe designs can deliver fluid at least 500 µm into agarose brain phantoms (1% w/v). This information is useful because reactive tissue responses typically radiate 500 µm around a neural prosthetic probe. Therefore it is possible for our probe design to deliver fluid to the necessary parameters. As a result, little if any modification needs to be made to our current probe designs.

The TRD results also provide an opportunity to characterize probes quantitatively. Using Nikon Elements software, we were able to calculate densitometry at three different locations along the probe (the shank, middle, and tip respectively) from the probe face to 500 µm away from the probe face, 500 data points per location per timepoint. With this ability, we were able to observe the densitometry vary at each location as time progressed. Given the vast number of images, (61 for every probe tested) we were not able to quantitatively analyze every timepoint. We selected 3 timepoints at one distance from the probe, 500 µm, that we thought would demonstrate the observable variance in densitometry most clearly (time = 0 minutes, 5 minutes, and 10 minutes). We extracted this data from each of the probe's recorded time-lapse images and analyzed it using Microsoft Excel. The results of this analysis are shown below (Figures 8-9).

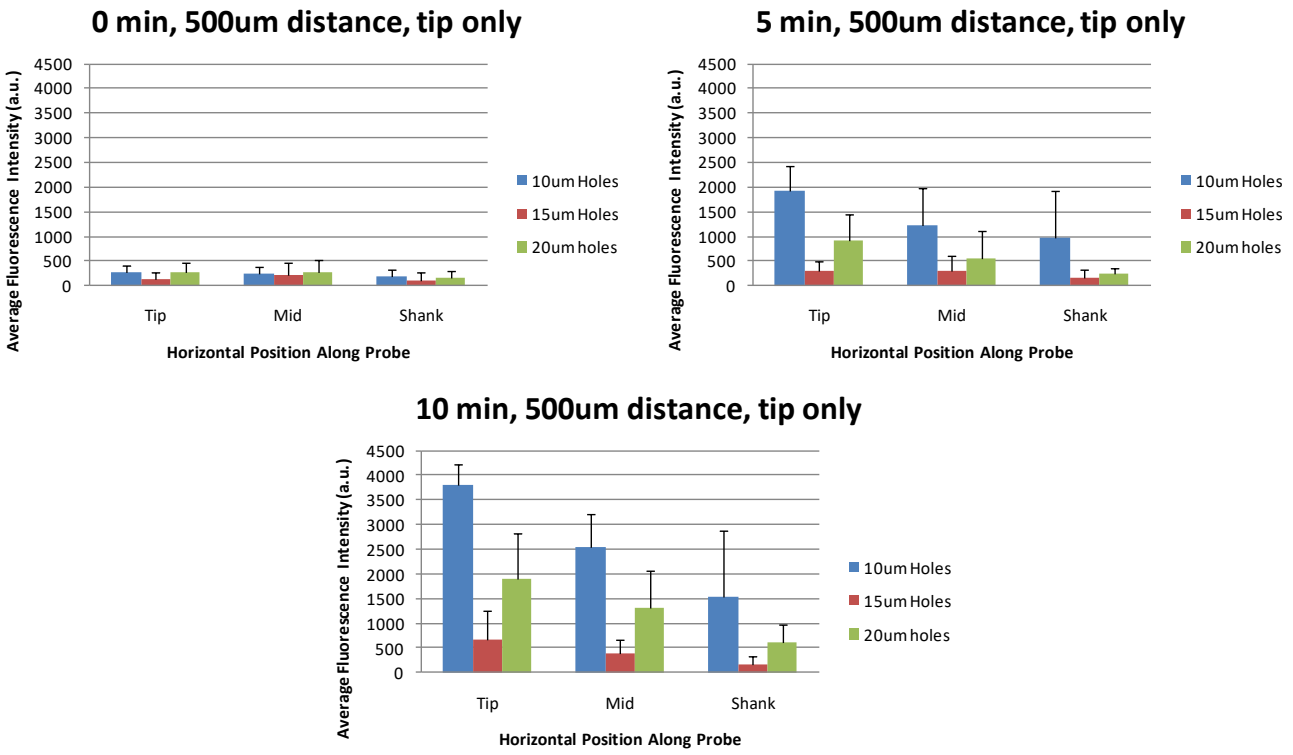

Figure 8. Comparison of fluorescence variance amongst probes with full-length geometries and either 10 µm, 15 µm, or 20 µm pores (see key). The graphed data represents the fluorescence intensity measured at 500 µm away from the probe face along its tip, middle, and shank. Fluorescence intensity was measured and extracted using Nikon Elements software. Error bars represent the standard deviation between at least 3 independent probe experiments for each condition.

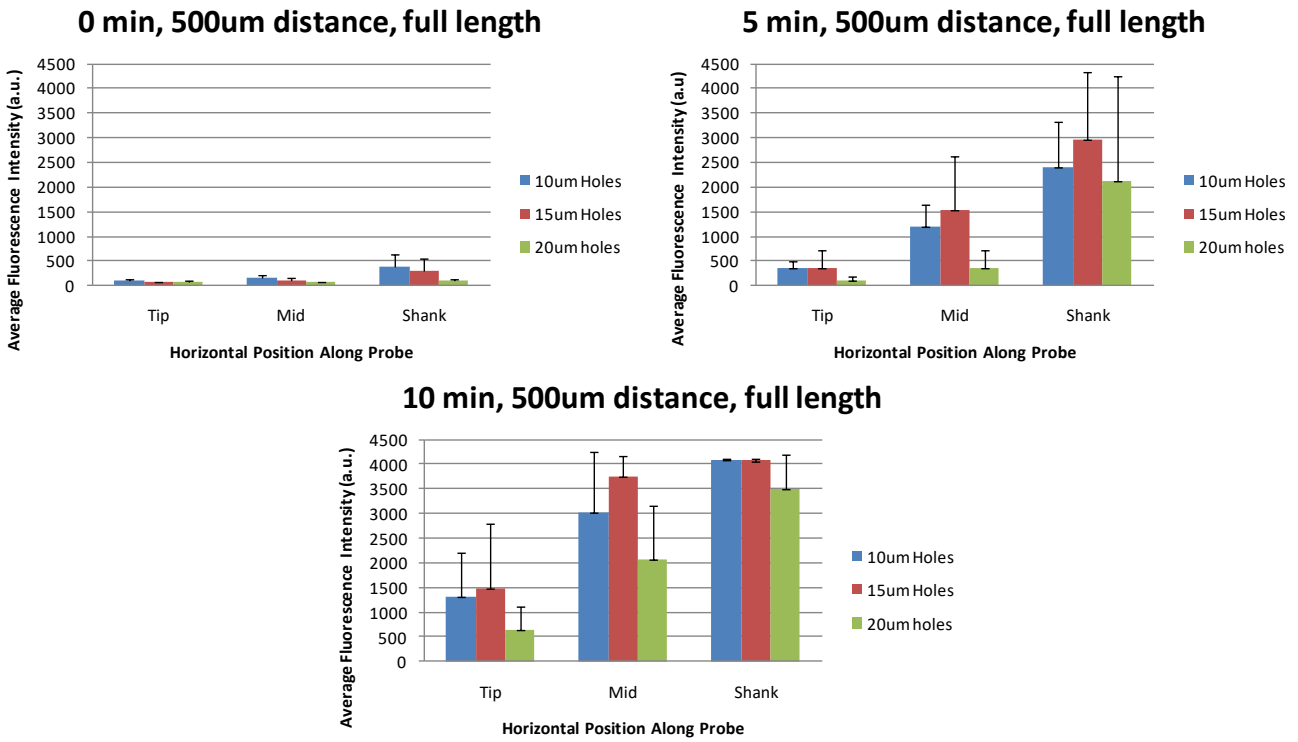

Figure 9. Comparison of fluorescence variance amongst probes with full-length geometries and either 10 µm, 15 µm, or 20 µm pores (see key). The graphed data represents the fluorescence intensity measured at 500 µm away from the probe face along its tip, middle, and shank. Fluorescence intensity was measured and extracted using Nikon Elements software. The tip of the probe is on the left side of each image, while the shank (connected with the polyimide tubing) is on the right side. Note: at 10 minutes along the probe shank 2 out 3 micropore sizes reach the limit of intensity, 4095 nm, thereby nullfiying the standard deviation.

These figures quantitatively demonstrate the qualitative observations from the CVS and TRD releases. Fluorescence intensity for probes with tip only geometries is highest at the tip, as expected. The charts also demonstrate our earlier qualitative observations. Larger micropores are associated with the release of more fluid. However, the overall trend of release in probes with tip only geometries is maintained regardless of micropore diameter; decreasing fluid release from the tip of the probe to the shank. Fluorescence intensity for probes is more consistent along the entirety of the probe. There is another substantial difference in geometries that the charts show; as time progresses pore size does not heavily influence fluorescence intensity for probes with full-length geometries. In the bottom graph in Figure 9, the fluorescence intensities for different pore diameters are relatively similar. This information

is critical when considering how to mediate immediate reactive tissue responses and should be given due consideration.

5. Conclusions

From previous work, it has been observed that reactive tissue responses radiate at least 500 µm from inserted neural probe device. The *in vitro* results from this study suggest that fluid delivery is possible past 500 µm with our probe design.

We observed that fluid delivery was most uniform from probes with a full-length geometry and 10 µm pores. Tip only geometries provided a more localized delivery relegated to the probe's tip and shank, while larger pore diameters yielded skewed delivery of fluid asymmetrically along the length of the probe. Specifically, full-length probes with larger pores, 20 µm, resulted in fluid delivery towards the shank (end connected to polyimide tubing) of the probes.

One caveat to these observations is that after 10 min of fluid delivery, Texas-Red dextran had diffused at least 500 um away from the probe along the entire length, regardless of geometry or hole diameter. These results indicate that all of the probes tested could be effective for delivery of drugs and/or siRNA to tissues during implantation. However, uniform distribution of fluid would be ideal to control overall dose of drug/siRNA delivered.

From these results, it may be possible for our current probe design to be utilized successfully in combating reactive tissue responses in their entirety. Furthermore, intervention can be mediated based on the probe geometry and/or pore diameter used. Consequently, a potential approach for handling reactive tissues' responses has been presented. Although this experiment represents the elementary stages of developing a viable clinical intervention strategy, the improvement of bio-compatibility and long-term stability of implantable neural prostheses seems possible.

The next logical step in this process is to attempt to correlate the *in vitro* results to *in vivo* results. If tat is accomplished, testing using siRNA delivery *in vivo* should commence.

6. References

1) Retterer, S., Smith, K., Bjornsson, C., Neeves, K., Spence, A. J., Turner, J., Shain, W., and Isaacson, M. *Model neural prostheses with integrated microfluidics: a potential intervention strategy for controlling reactive cell and tissue responses.* IEEE Trans Biomed Eng, 2004. 51(11): p. 2063-2073.

2) Hoogerwerf, A.C. and Wise, K.D. *A three-dimensional microelectrode array for chronic neural recording.* IEEE Trans Biomed Eng, 1994. 41(12): p. 1136-46.

3) Oh, S.J., et al. *Regional differences of reactive responses against silicon neural probe implanted into deep brain regions.* Society for Neuroscience, 2003.

4) Biran, R.., D.C. Martin, and P.A. Tresco, *Neuronal cell loss accompanies the brain tissue response to chronically implanted silicon microelectrode arrays.* Exp Neurol, 2005. 195(1): p. 115-26.

5) Dirnagl, U., Iadecola, C., and Moskowitz, M.A. *Pathobiology of ischaemic stroke: an integrated view.* Trends Neurosci, 1999. 22(9): p. 391-7.

6) Anderson, R.E., et al. *Biochemical markers of cerebrospinal ischemia after repair of aneurysms of the descending and thoracoabdominal aorta.* J Cardiothorac Vasc Anesth, 2003. 17(5): p. 598-603.

7) Turner, J.N., et al. *Cerebral astrocyte response to micromachined silicon implants.* Exp Neurol, 1999. 156(1): p. 33-49.

8) Szarowski, D.H., et al. *Brain responses to micro-machined silicon devices.* Brain Res, 2003. 983(1-2): p. 23-35.

9) Merrill, D.R. and Tresco, P.A. *Impedance characterization of microarray recording electrodes in vitro.* Conf Proc IEEE Eng Med Biol Soc, 2004. 6: p. 4349-52.

10) Rousche, P.J. and Normann, R.A. *Chronic recording capability of the Utah Intracortical Electrode Array in cat sensory cortex.* J Neurosci Methods, 1998. 82(1): p. 1-15.

11) Williams, J.C., Rennaker, R.L., and Kipke, D.R. *Long-term neural recording characteristics of wire microelectrode arrays implanted in cerebral cortex.* Brain Res Brain Res Protoc, 1999. 4(3): p. 303-13.

12) Nichols, A.M., et al. *A screw microdrive for adjustable chronic unit recording in monkeys.* J Neurosci Methods, 1998. 81(1-2): p. 185-8.

13) Spataro, L., Dilgen, J., Retterer, S., Spence, A., Isaacson, M., Turner, J., and Shain, W. *Dexamethanose Treatment Reduces Astroglia Responses to Inserted Neuroprosthetic Devices in Rat Neocortex.* J. Neuroscience. (submitted)

14) Shain, W., Spataro, L., Haberstraw, K., Dilgen, J., Retterer, S., Spence, A., Isaacson, M., and Turner, J. *Controlling cellular reactive responses around neural prosthetic devices using peripheral and local intervention strategies.* IEEE Trans. Rehab. Eng., 2003. 11 (2), pp.186-188.

15) Merck Sharp & Dohme Corp., Initials. *Science and technology*. http://www.sirna.com/science_technology/index.html, 2007.

16) Hynd, M. *Probe Research Strategy*. State University of New York at Albany. 2009.

17) Lewis, S.L., Heitkemper, M.M., Dirksen, S.R., O'Brien, P.G., and Bucher L. *Medical Surgical Nursing: Assessment and Management of Clinical Problems*. 2008.

18) Gracias, X, Feng, B. Xu, and Castracane, J. *Journal of Microlithography, Microfabrication, and Microsystems.* 5, 021102.